Revival of legacy land seismic surveys using advanced processing technologies: an example from the Carpathian foothills

Adrien Meffre[1*], Vincent Prieux[1], Matthieu Retailleau[1], David Le Meur[1], Abel Afonso Monteiro[1], Zied Bouzouita[1], Fang Wang[1], Sofia Mestiri[1], Tünde Markos[3], Justin Vermeulen[2], Jozsef Orosz[3] and Emma Tyler[2] review the key processing and imaging steps helping to revive legacy land seismic surveys in a structurally complex area.

Introduction

The Getic Depression is located to the south of Romania and represents the foothills of the Southern Carpathians with a low relief (from 100 to 450 m), cut by river valleys and covered with forests and cultivated fields (Figure 1a). While the eastern part of the Getic Depression is interpreted as the continuation of the Eastern Carpathians, the western part of the Getic basin corresponds to a thrust area between the Carpathians and the Moesian platform. This basin is a mature petroleum area with thousands of wells drilled and several fields discovered since exploration started a century ago. In the past 15 years, several 3D narrow-azimuth seismic surveys have been recorded to increase knowledge of the geology of the subsurface with the ultimate aim of optimizing production from Tertiary and Jurassic clastic reservoirs. These surveys were acquired with different acquisition geometries and different types of seismic source (dynamite, vibroseis or airguns). The seismic data sets were independently processed in either the time or depth domain. As shown in Figure 2, a composite time section of the legacy seismic volumes shows considerable inconsistency in amplitude, signal-to-noise ratio (S/N) and continuity of the main geological features. In 2019, OMV Petrom initiated the reprocessing of these surveys as a single merged depth volume. In this paper we review the key processing and imaging steps helping to revive legacy land seismic surveys in this structurally complex area.

Input seismic data

The input data consist of 12 land seismic surveys, with small overlaps between them. In total, seismic data of over 2447 km^2 were acquired from 2006 to 2014. Acquisition was challenging in this area due to the presence of villages, rivers, lakes, as well as cultivated and industrial areas. As shown in Figure 1b, dynamite was the main source, representing 87% of the recorded

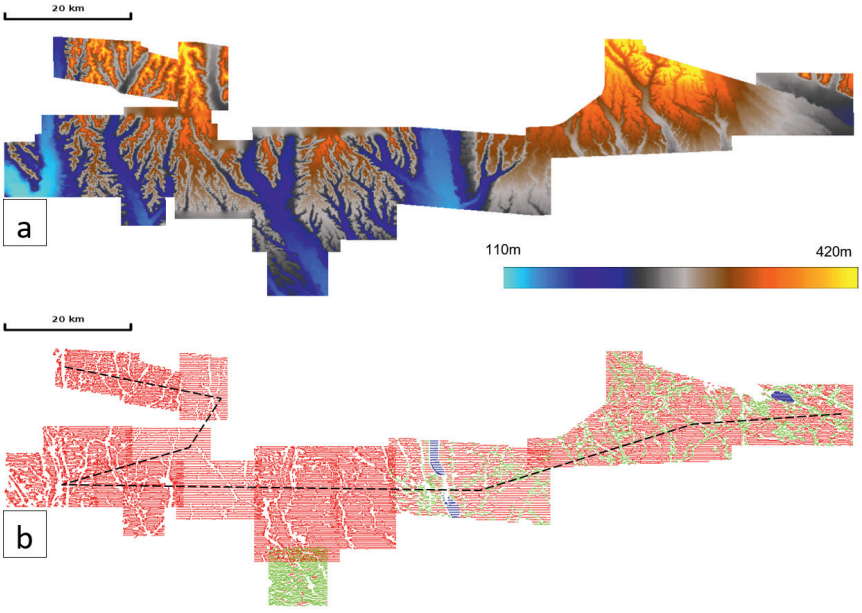

Figure 1 a) Topographical map of the Getic area in the southern part of Romania with a low relief cut by several valleys. b) Map of the original shot positions from the 12 surveys. Dynamite source in red, vibroseis in green and airguns in blue. The dashed line corresponds to the composite seismic section through all the legacy surveys shown in Figure 2.

[1] CGG | [2] OMV PETROM | [3] OMV E&P
[*] Corresponding author, E-mail: adrien.meffre@cgg.com
DOI: 10.3997/1365-2397.fb2022002

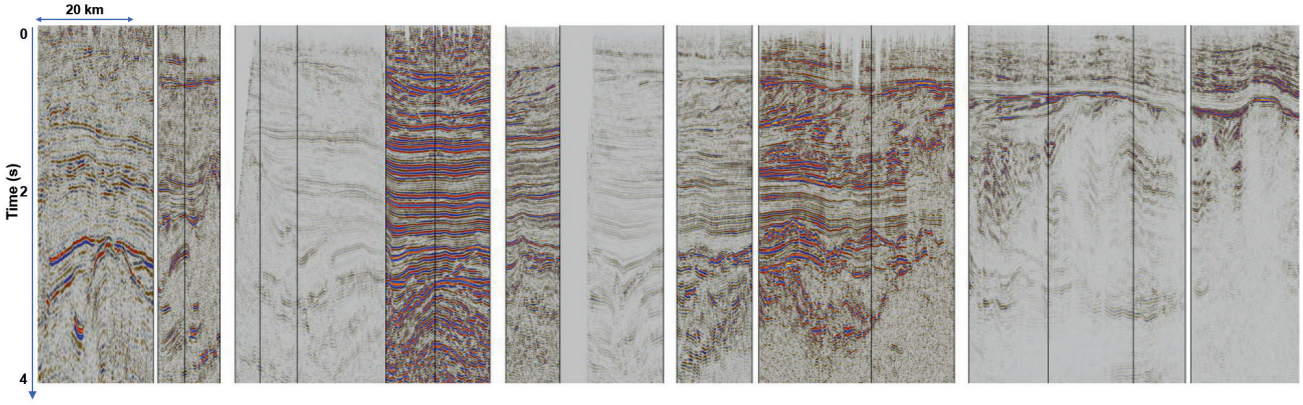

Figure 2 Composite time section through all legacy volumes shows a significant inconsistency in amplitude and continuity of the main geological features.

shots. However, a vibroseis source with a sweep frequency from 8 to 80 Hz was also used in accessible areas and represented 12% of shot points. Airguns were deployed on the lakes and rivers (only 1% of recorded shots). These narrow-azimuth surveys were acquired using a sparse orthogonal configuration in the same direction (East-West) as the shot lines (Figure 1b). The acquisition parameters were significantly different from one survey to another: the receiver line intervals were from 200 to 450 m; the source line intervals were from 300 to 450 m with many holes; the shot and receiver station intervals also varied from 35 to 50 m. On average, the bin size of the common midpoint (CMP) was 25 m by 25 m with a nominal fold of 60 and maximum offset of 3500 m.

Signal processing

Surface wave attenuation with primary protection

The first challenge faced by this reprocessing was attenuation of the strong surface waves which were generally aliased above 8 Hz for all the surveys. This was mainly due to the sparse acquisition used, as described above. In order to build a high-fidelity ground-roll model, we first estimated frequency-variant phase velocities of the surface waves (Le Meur et al., 2008) in order to regularize and densify the raw data in the cross-spread domain using a joint low rank and sparse inversion approach (Sternfels et al., 2016).

A data-driven interferometry method was then used to build the surface-wave model (Chiffot et al., 2017) which was then adaptively subtracted from the raw data. To minimize damage to the primary reflections and diffractions, a primary model was used in the adaptive subtraction workflow. The primary model was built by a depth demigration of a reflectivity volume, which was derived from a pre-stack depth migration with preliminary noise attenuation applied. This iterative approach allowed an effective attenuation of the surface waves while minimizing signal leakage and preserving diffractions. This workflow was applied on all individual surveys with adapted parameters and the results are shown in Figures 3a-b. The time slice through all surveys on the right-hand panel shows the effective attenuation of the different acquisition imprints and aliased surface waves. The time section demonstrates the possibility of recovering weak high-frequency primary reflections and diffractions masked by strong aliased low-frequency ground-roll.

Signal harmonization through survey merging

The second challenge after noise attenuation was to address the signal inconsistency across the different surveys acquired with different sources and receivers. To achieve this, we first needed to correct the effects of near-surface variations that distorted the recorded signal in amplitude, phase and time. Surface-consistent algorithms were used to compute amplitude scalars and deconvolution operators for each shot and receiver (Garceran and Le Meur, 2012,). All datasets from the 12 surveys were analysed simultaneously to retrieve the signature of 33 different sources to correct amplitude and phase distortions for every shot and receiver. We computed surface-consistent zero-phase spiking deconvolution operators which produced a stable, broadband signal that matched the well synthetic logs especially at low frequencies. Then, residual reflection statics were computed in one pass for all the surveys, through a stochastic approach proposed by Le Meur and Poulain (2011,), in order to improve continuity and focusing of reflections. Finally, an application of 5D anti-leakage regularization and interpolation, as proposed by Poole (2010), yielded a continuous set of azimuth gathers regularly sampled in the x and y offset dimensions whilst also filling any gaps from irregular acquisitions (Figure 3c). The time-migrated section on the left shows the continuity of the clinoforms (black arrows) and a sharp definition of the faults in the thrust area. On the time slice, the continuity of the geological features as nappes or clinoforms is improved (zoom areas on Figure 3c, right).

Depth velocity model building

Updating the near-surface velocity model

The third challenge related to building a depth near-surface velocity model. The main difficulty lay in taking into account the highly variable topography with the presence of very low velocities in the weathering zone. Despite recent advances in onshore depth imaging technology (Sedova et al., 2019), the low-velocity layer was extremely difficult to capture. Reflection tomography suffered from insufficient data at near angles and poor S/N while refraction tomography and diving-wave full-waveform inversion (FWI) were impeded by illumination gaps in the presence of strong velocity inversions.

The very low velocities and the strong lateral velocity gradient can usually be recovered through multi-wave inversion (MWI) by simultaneously utilizing the frequency-variant phase velocity of the surface waves and the first-break picks (Bardainne,

2018; Prieux et al., 2020). The quality of the surface waves varies significantly across different surveys as shown on dispersion spectra (Figure 4a). To improve the continuity of the fundamental mode of the surface waves on dispersion panels, offline processing was performed to compute accurate frequency-variant picks for each pair of source-receivers on all the surveys (Donno et al., 2021). This workflow paved the way for MWI to use all the picks from all individual surveys to retrieve the complexity of the near-surface and minimize edge effects at survey boundaries (Figure 4b-c). Then the updated P-wave velocity from MWI was integrated into the initial depth P-wave velocity model for a joint reflection/refraction tomography (Allemand et al., 2017), which

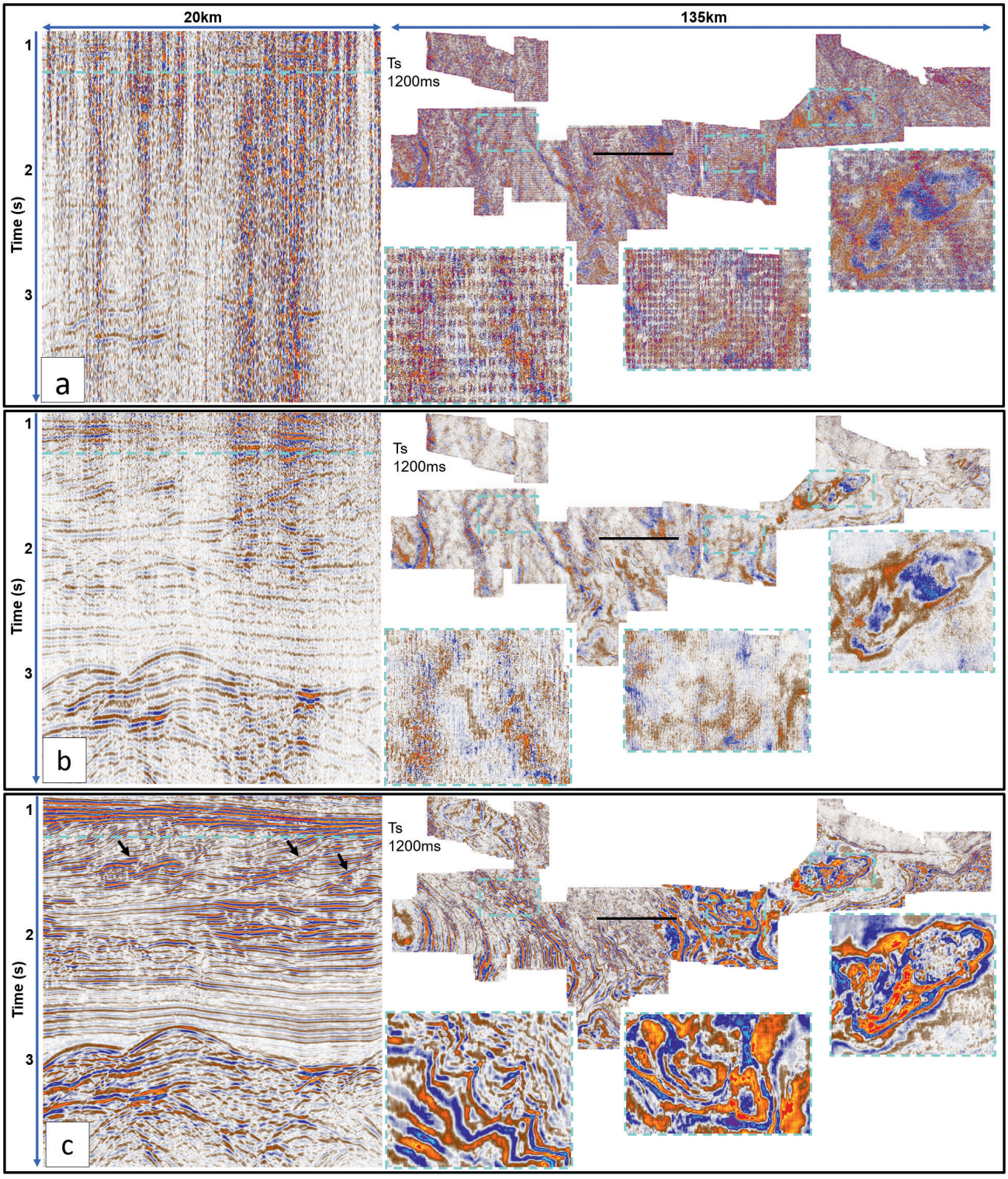

Figure 3 Time section (located on the black line on the time slice) and time slice (with three zooms) at 1200 ms (cyan dashed line on the time section), extracted from a) the raw data, b) the processed data after noise attenuation and c) after signal harmonization for all the surveys. The raw data contain strong aliased surface-wave imprints that mask the reflections from top to bottom. The noise attenuation allows recovery of the continuity of geological events. The signal harmonization achieves a better focusing and fault delineation in the clinoform (see time section), while improving the stability of the signal across the disparate surveys (see time slice).

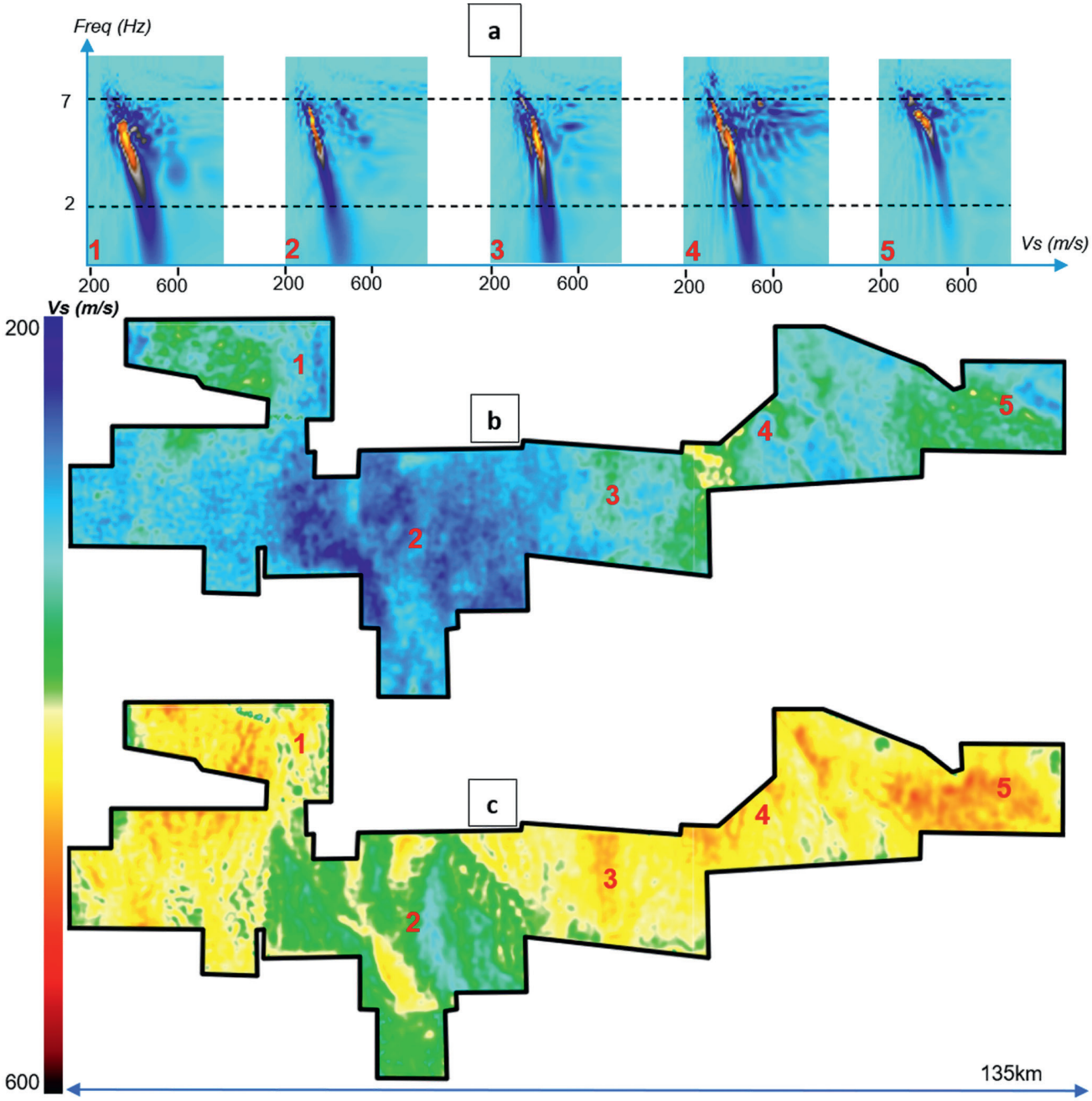

Figure 4 (a) These phase velocity frequency spectra illustrate the dispersive nature of the surface waves with decreasing velocity as the frequency increases across the whole survey. (b) and (c) are the result of surface-wave tomography for frequencies 3 Hz and 7 Hz respectively. These maps clearly reveal the heterogeneity of the near surface on the whole survey with minimal artefacts at survey boundaries.

used the picks from the residual move-out (RMO) and the first breaks to update the shallow P-wave velocity and anisotropy models.

The benefit of this dedicated workflow is demonstrated on Kirchhoff depth-migrated sections as shown in Figure 5. Imaging distortions due to strong near-surface velocity variations were well corrected from the surface down to the deeper targets (white arrows) owing to the improved lateral and vertical resolution of the near-surface velocity model, despite strong topography.

Challenges of velocity model building

The south of the Romanian Carpathian Mountains is characterized by an important thrust inclusion in the north of the merged surveys which is inserted inside the younger sediments of the Getic basin, as described by Krezsek et al. (2011). This intrusion is the result of regional compressional constraints applied to the Getic foreland basin, occurring from the Eocene-Burdigalian until the Mid-Sarmatian. The so-called Burdigalian wedge shifted into the Getic basin along the Burdigalian salt detachment on top of the Moesian platform. The frontal part of the Burdigalian wedge is then an imbricate slice of the Upper Burdigalian strata.

The geological complexity poses numerous challenges to seismic imaging. The thrust sediments are characterized by a very complex structure with steep dips, strong lateral and vertical velocity variations with some high velocities. If this complexity is not properly resolved, the resulting image presents a very

low local reflectivity, some strong deformations of its base and the reflectors below it (see the red arrows in Figure 6d). As the velocities of sediments below the thrust are notably slower than those in the thrust, this causes a strong velocity inversion at the base of the thrust (Figure 6b). It is particularly important that the velocity contrasts accurately delineate the complex shape of the thrust body to avoid imaging distortions beneath. Furthermore, the tectonic history of the area is the cause of significant faulting and compressional/extensional stresses, which in turn cause horizontal transverse isotropy (HTI) anisotropy i.e., azimuthal velocity variations, and consequently lead to imaging issues when not properly handled.

Building a detailed and complex velocity model through multi-layer tomography

The fourth challenge involved the building of a depth velocity model containing multiple heterogeneous layers with high-velocity contrasts identified in the well sonic logs. Therefore, the velocity model was firstly updated through the multi-layer (ML) tomography approach, as proposed by Guillaume et al. (2012). The advantage of this approach is the ability to perform a global update of several layers simultaneously while updating the layer boundaries and naturally preserving the velocity contrasts at the boundaries. Because of the complexity of the thrust body, the high uncertainty of the starting model, the heterogenous reflectivity with

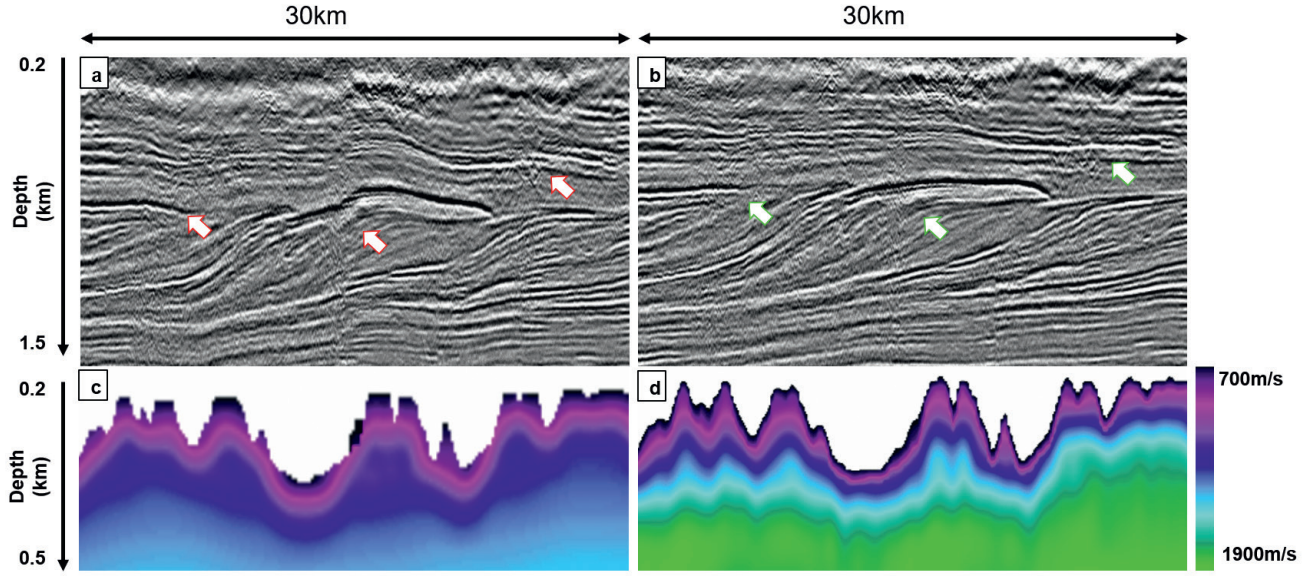

Figure 5 (a-b) Stack after Kirchhoff pre-stack depth migration (PSDM) and (c-d) near-surface velocity models built from (c) a smooth time tomography and (d) an MWI and joint reflection/refraction tomography respectively. This last model includes a very low velocity at 700 m/s in the first shallow layer. The green arrows (b) show the significant reduction in the distortions due to inaccurate near-surface velocity model.

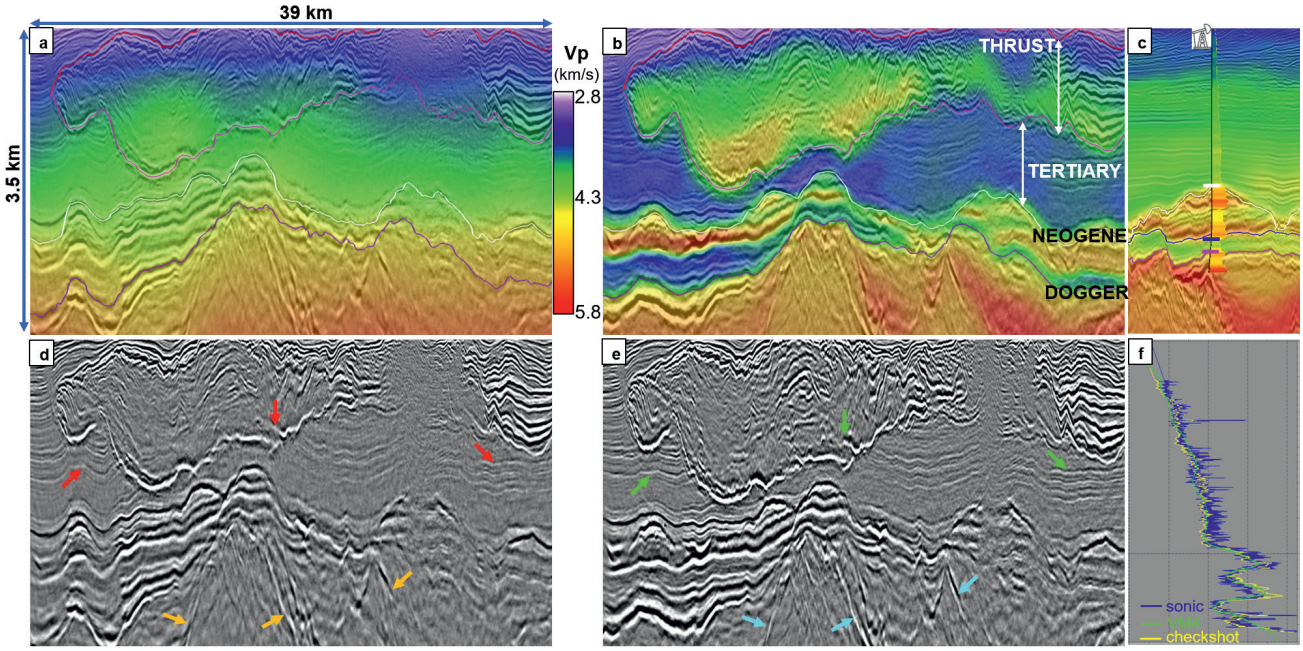

Figure 6 Velocity model superimposed on the corresponding Kirchhoff Pre-Stack Depth Migration (PSDM) stack (a) after the first tomographic update and (b) with the final velocity model. Note the strong velocity contrasts inside and around the thrust. (d, e) Kirchhoff PSDM stacks after the first and final tomographic updates respectively. (c, f) Comparison between the sonic and the final velocity profile (different line from the section in (a-b)). In (c), a good match is seen between the depth of well markers and the horizon map migrated in the final model.

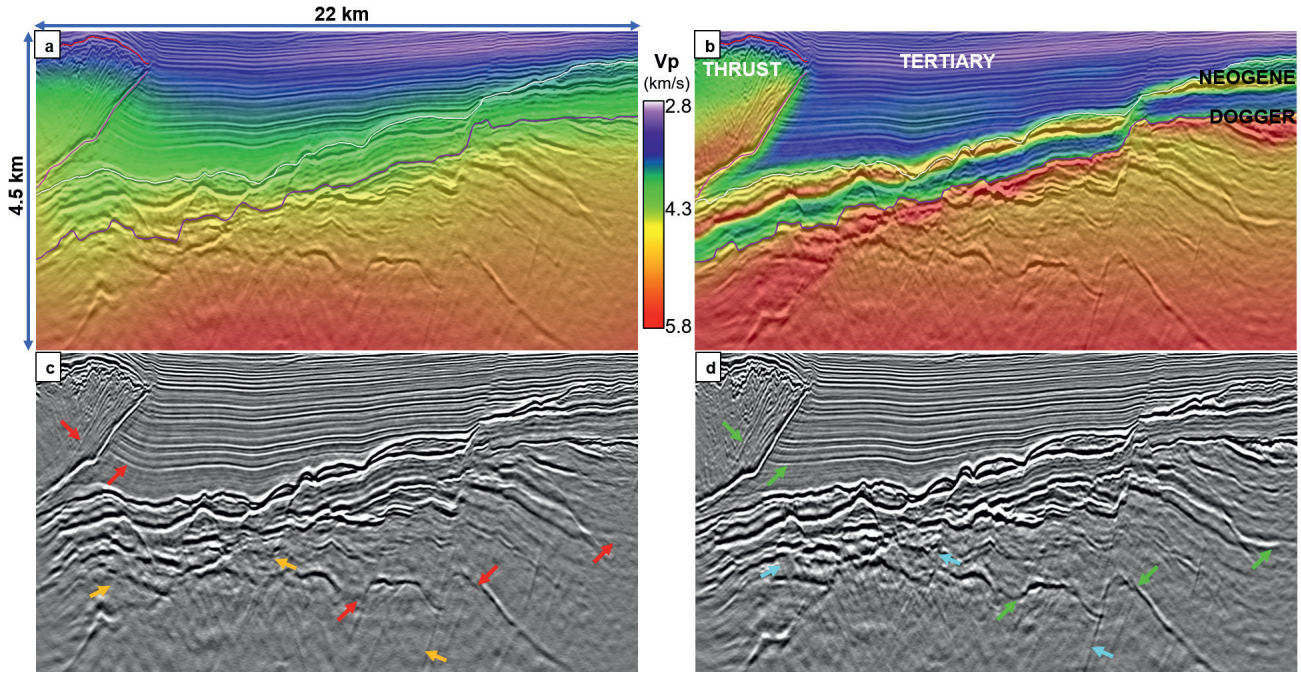

Figure 7 (a-b) Velocity model superimposed on the corresponding Kirchhoff PSDM stack, and (c-d) Kirchhoff PSDM stacks, after the first tomographic update (a, c) and with the final velocity model (b, d). We can see the simplification of the structure below the thrust (green arrows) and the better definition of the faults (blue arrows).

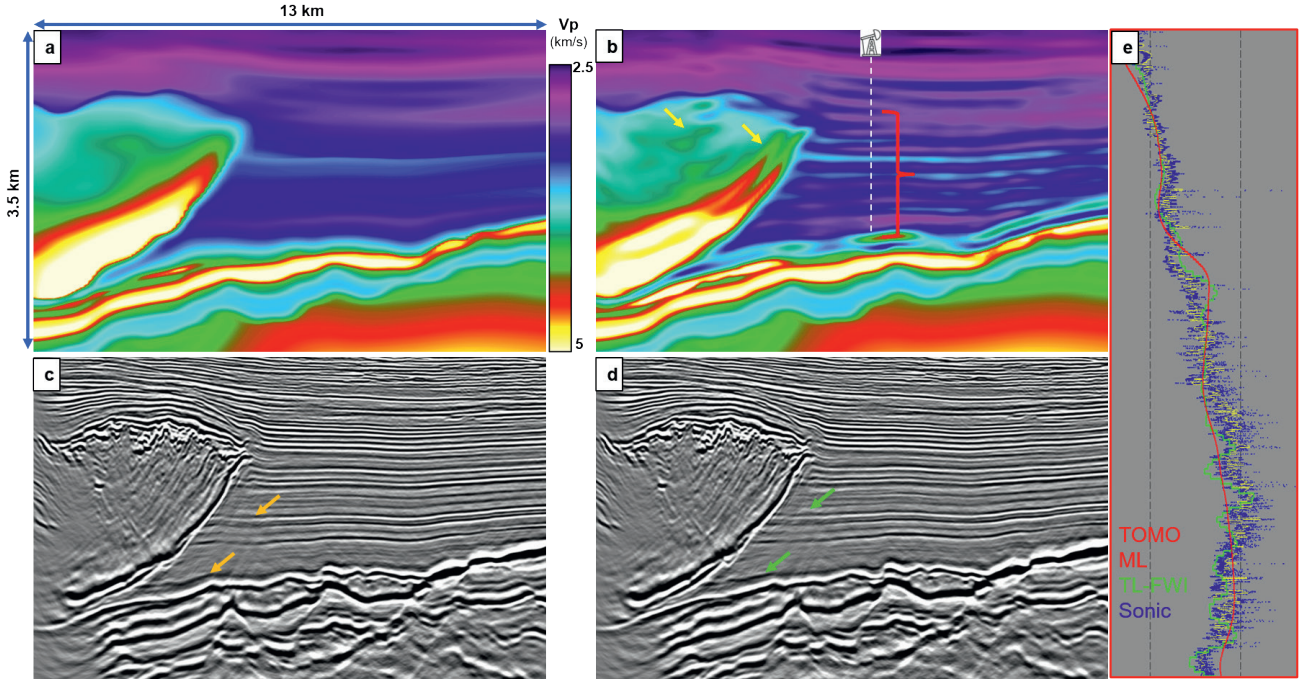

Figure 8 Subline section of (a) output of ML tomography and (b) output velocity model from TL-FWI, and their corresponding Kirchhoff PSDM images (c) and (d). It is observed that the velocity model from TL-FWI nicely fits the well sonic logs (e).

the poor quality of the RMO picks and the limited offset to 3500 m, it was very difficult to use a conventional iterative ML tomography workflow to obtain an accurate velocity model. A joint stack and gather scanning tomography, as proposed by Gong and Wu (2018), was therefore implemented to improve the starting model. Initially, we generated PSDM stack images by velocity scanning and selected the best images in terms of structure and focusing, such that the large spatial wavelengths of the velocity were updated. Secondly, a gather scanning tomography was implemented, in which the RMO picks estimated from all the different velocity percentage models were jointly used. With this step, we were able to update velocities with a medium wavelength and further improve the focusing of the images, as shown in Figures 6 a-b and 7 c-d (green arrows below the thrust). During the initial model building, it was important to incorporate the well information into the definition and resolution of the velocity model. At this stage, collaboration with interpreters was crucial to build a geologically conformable velocity model using the well information. The velocity extrapolation and its calibration were performed layer by layer, to ensure that the extrapolated velocities and contrasts were consistent with the well

markers (Figure 6c). The resulting model thus contained strong velocity contrasts and velocity inversions as visible in the wells at the correct depths (Figure 6f). Finally, this model was used as the initial model in the high-definition ML tomography, which used dense RMO picks with wide-azimuth to perform so-called 'multi-dip picks', where the structural dips were measured and demigrated separately for each azimuth and offset class (Reinier et al., 2021). By adding a better resolution of the velocity field inside the thrust, it was possible to simplify the geological structure of the reflectors below. The major faults structuring the basement below the Dogger are better defined and sharper and with a more plausible geological orientation in the final model, as highlighted by the blue arrows (Figures 6e and 7d).

High-definition velocity model through Time-Lag Full-Waveform Inversion (TL-FWI)

The strong high-frequency (HF) velocity variations inside the thrust are very challenging to capture even with high-definition ML tomography. Small residual distortions were visible below the thrust (Figure 8a, c). Full-waveform inversion (FWI) is a natural way to derive the best possible velocity model for pre-stack depth migration. The TL-FWI approach proposed by Zhang et al., (2018), was performed in addition to the ML tomography in order to better use the full reflection data and therefore improve the accuracy and resolution of the velocity model despite the limited offset range (3 km). These HF vertical velocity variations were able to resolve most of the residual distortions visible on seismic events underneath the thrust, as shown by the yellow arrows in Figure 8 c-d.

Depth imaging results

Legacy comparison

To highlight the benefits of our reprocessing with the most advanced depth imaging algorithms, we compared our final tilted transverse isotropy (TTI) Kirchhoff PSDM (Figure 9) with the legacy result generated from a post-stack match and merge

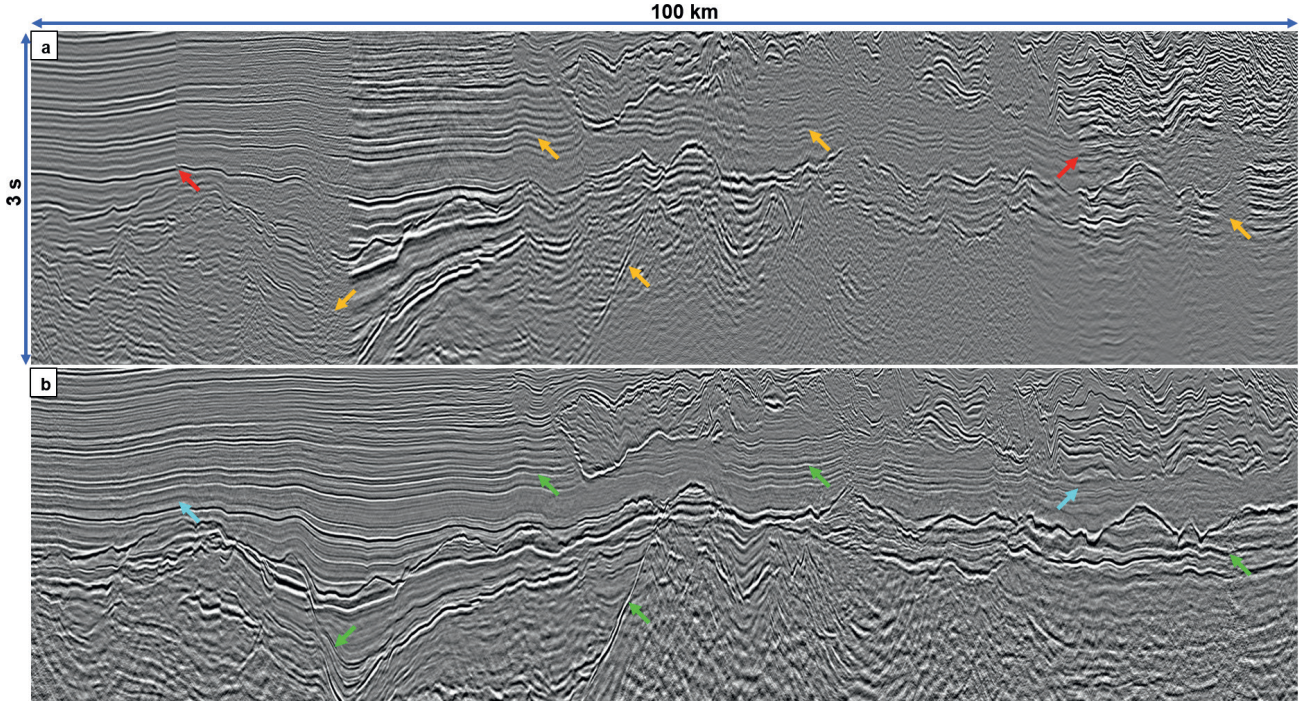

Figure 9 Comparison in the time domain: a) legacy PSTM stack, b) TTI Kirchhoff PSDM stack with our final velocity model. The latter presents an improved reflectivity and continuity of the reflectors with a broader frequency content. The distortions below the thrust are better resolved (green arrows) and the imaging of the pre-Neogene unit is much improved with sharper fault definition (cyan arrows).

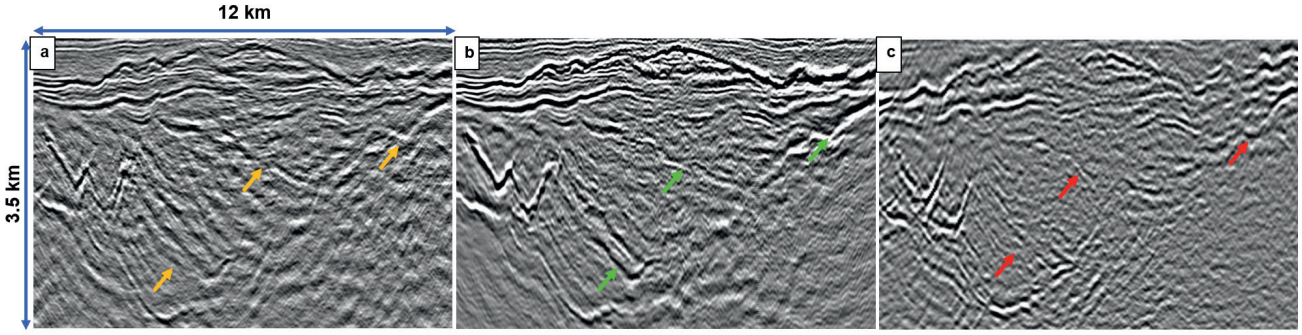

Figure 10 Comparison in time of: (a) Kirchhoff PSDM and (b) RTM PSDM stack using the same final velocity model with c), legacy PSTM stack. More coherent events, a better focusing of the deep events and less migration smiles are obtained with the RTM approach (green arrows). Both PSDM results (Kirchhoff and RTM) are better than the legacy PSTM result (orange and red arrows respectively).

of all the individual surveys. The new volume shows a clear enhancement of the final PSDM image. The seismic resolution of the main geological structures and their interpretability are drastically improved throughout all the individual surveys, as highlighted by the green arrows in Figure 9b. The continuity of events and the increased S/N across the whole merged survey with a broader frequency content benefit the geological interpretation and reservoir characterization. We also note the improved reflectivity and continuity of the base of the thrust and the reduction in distortion below it, as well as a sharper definition of the faults (green arrows in Figure 9b).

Reverse time migration

The final challenge was how to better utilize the strong and complex velocity contrasts in our final velocity field, especially in the deeper section with strong velocity variations in the overburden. To achieve this, a reverse time migration (RTM) was performed (Zhang and Zhang, 2011). The RTM generated vector offset output (VOO) gathers consisting of azimuth and offset classes (Agnihotri et al, 2015). By further processing the VOO gathers, an enhanced RTM VOO imaging was obtained. Time comparisons of the Kirchhoff PSDM stack, the enhanced PSDM RTM VOO image below the Neogene layer, and the legacy PSTM image are shown in Figure 10. Compared to the Kirchhoff image, the RTM algorithm can better manage the complexity and the strong velocity contrasts of the model. The RTM better focuses the thin reflectors in the reservoir area and better images the shape of the steeper dipping structures in the deep (green arrows in Figure 10b).

Conclusion

This paper demonstrates that applying the latest processing and imaging technologies significantly increases the value of legacy land surveys, especially in a challenging context characterized by limited fold, diverse and sparse acquisition geometries, and a structurally complex thrust area with strong velocity contrasts. Obtaining a consistent depth image across the surveys can help to improve regional structural understanding and reservoir characterization. This objective was achieved by applying high-end algorithms in pre-processing, such as efficient surface wave attenuation while preserving the signal by using primary protection, and signal harmonization through surface-consistent methods and 5D interpolation when merging surveys. We then built the depth velocity model from top to bottom starting with an update of the near-surface velocity model taking into account a highly variable topography. The final velocity model in such a complex geological setting was obtained with a dedicated tomography and full-waveform inversion workflow. Finally, by applying an advanced migration such as reverse time migration we could benefit from this complex model to capture very steep structures and better focus weak seismic events. The application of advanced processing and depth imaging technologies helps to revive legacy land seismic surveys in complex geological areas where obstacles, protected natural areas or recent residential locations make it difficult to acquire modern seismic data.

References

Allemand, T., Sedova, A. and Hermant, O. [2018]. Flattening common image gathers after waveform inversion: the challenge of anisotropy estimation, 88th Ann. Internat. Mtg.: Soc. of Expl. Geophys.

Agnihotri, Y., Wu, Q. and Xu, D. [2015]. Salt delineation using vector offset output (VOO) of full azimuth data. GCAGS - Gulf Coast Association of Geological Societies (Houston, USA).

Bardainne, T. [2018]. Joint inversion of refracted P-waves, surface waves and reflectivity, 80th Eur. Ass. Geosc. Eng., Extended Abstracts.

Chiffot, C., Prescott, A., Grimshaw, M., Oggioni, F., Kowalczyk-Kedziers-ka, M., Cooper, S., Johnston, R. and Le Meur, D. [2017]. Data-driven interferometry method to remove spatially aliased and non-linear surface waves, 87th Ann. Internat. Mtg.: Soc. of Expl. Geophys.

Donno, D., Farooqui, S., Mostafa, K., McCarthy, D., Solyga, D., Courbin, J., Prescott, A., Delmas, L. and Le Meur, D. [2021]. Multiwave inversion: A key step for depth model building – examples from the Sultanate of Oman: *The Leading Edge*, August issue, 610-618.

Garceran, K. and Le Meur, D. [2012]. Simultaneous Joint Inversion for Surface Consistent Amplitude and Deconvolution: 74th Eur. Ass. Geosc. Eng., Extended Abstracts.

Gong, Z. and Wu, X. [2018]. Non-linear scanning tomography for velocity model building in seismic-obscured area. Anaheim, 88th Ann. Internat. Mtg.: Soc. of Expl. Geophys.

Guillaume, P., Hollingworth, S., Zhang, X., Prescott, A., Jupp, R. and Pape, O. [2012]. Multi-layer tomography and its application for improved depth imaging. 82th Ann. Internat. Mtg.: Soc. of Expl. Geophys.

Krezsek, C., Oterdoom, H., Dzido, P., Barbu, V., Bland, S., Arnberger, K. and Lapadat, A. [2011]. New insights into the hydrocarbon system of the getic Depression Romania: Implicationsfor Exploration, 73rd Eur. Ass. Geosc. Eng., Extended Abstracts.

Le Meur, D. and Poulain, G. Monte-Carlo [2011]. Statics on Large 3D Wide-Azimuth data. 73rd Eur. Ass. Geosc. Eng., Extended Abstracts.

Le Meur, D., Benjamin, N., Cole, R. and Al Harthy, M. [2008]. Adaptive Groundroll filtering. 69th Eur. Ass. Geosc. Eng., Extended Abstracts.

Poole, G. [2010]**.** 5D data reconstruction using the anti-leakage Fourier transform. 72nd Eur. Assn. Geosci. Eng, Extended Abstracts

Prieux, V., Bardainne, T., Meffre, A., Prigent, H., Van Kleed, F.J., Waqas, M. and Hou, L. [2020]. Structurally constrained anisotropic Multi-Wave Inversion utilizing Machine Learning and Big Data on a Middle East OBC project. 82nd Eur. Assn. Geosci. Eng, Extended Abstracts.

Reinier, M., Allemand, T., Salaun, N., Yu, Z., Pouget, M., Henry-Baudot, A., Chaintreuil, B., Mihoub, M., Gigou, G. and Espin, I. [2021]. Resolving small scale lateral velocity anomalies without FWI or stochastic approaches, 83rd Eur. Assn. Geosci. Eng, Extended Abstracts.

Sedova, A., Royle, G., Allemand, T., Lambaré, G. and Hermant, O. [2019]. High-frequency acoustic land full-waveform inversion: a case study from the Sultanate of Oman: *First Break*, vol **37**(1), Jan. 2019, pp. 75–81.

Sternfels, R., Prescott, A., Pignot, G., Tian, L. and Le Meur, D. [2016]**.** Irregular spatial sampling and rank reduction: interpolation by joint low-rank and sparse inversion, 78th Eur. Assn. Geosci. Eng, Extended Abstracts.

Zhang, H. and Zhang, Y. [2011]. Reverse Time Migration in Vertical and Tilted Orthoreombic Media, 81st Ann. Internat. Mtg.: Soc. of Expl. Geophys.

Zhang, Z., Mei, J., Lin, F., Huang, R. and Wang, P. [2018]. Correcting for salt misinterpretation with full waveform inversion: 88th Ann. Internat. Mtg.: Soc. of Expl. Geophys.